THE JOURNAL OF PHYSICAL CHEMISTRY C

pubs.acs.org/JPCC Article

σ-Aromaticity in the MoS_2 Monolayer

Maksim Kulichenko and Alexander I. Boldyrev*

Cite This: J. Phys. Chem. C 2020, 124, 6267−6273 Read Online

ACCESS | Metrics & More | Article Recommendations | Supporting Information

ABSTRACT: Molybdenum disulfide is a prominent semiconductor that received a lot of attention recently due to its unique properties. Possessing a layered crystal structure, one can tune the band gap from indirect to direct while transforming the material from the bulk to monolayer structure. MoS_2 is a highly researched material. However, not all of the nature of this intriguing material is revealed yet. The aim of this work is to deepen the knowledge of the scientific community about MoS_2 by deciphering its bonding picture. As is shown using the SSAdNDP approach, Mo and S form 2-centered bonds and there is a lone pair on each S. Most importantly, the remaining electrons are distributed over Mo atoms and form conjugated aromatic σ-bonds inside every hexagonal ring, which makes molybdenum the main carrier of σ-aromaticity.

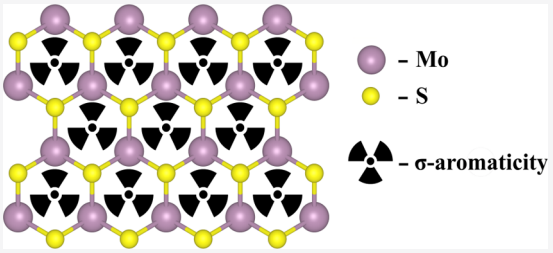

1. INTRODUCTION

Nowadays, the development of materials with tunable electronic and mechanical properties is a topical task in the field of nanoscience. The recent progress of experimental and theoretical techniques allows the fabrication and characterization of monolayer- and few-layer-scale structures that obtain different and unique properties as they transform from bulk to nanostructures. The need of the nanotechnology industry for materials with desired properties is partially covered by transition metal dichalcogenides. Transition metal dichalcogenides (TMDs) form a big class of layered compounds with the general formula MX_2, where M stands for a transition metal, and X is a chalcogen. The neighboring layers interact via weak van der Waals forces,[1] while M and X atoms within one layer have strong covalent bonding.[2,3] TMD materials have been widely explored recently,[4−12] and amidst them, molybdenum disulfide (MoS_2)[13−18] received the most attention of researchers from different chemical and physical disciplines. The configuration of stacked layers exhibits properties of a dry lubricant, which found an application in aerospace technologies.[19,20] Besides its outstanding mechanical characteristics, this layered material has the ability to transform from an indirect band gap of 1.2 eV in bulk to a direct band gap of 1.9 eV in the monolayer.[21,22] Due to its unique electronic[23−31] and optical[18,32] properties including tunable band gap,[16,33,34] MoS_2 is one of the most intensively studied materials in the world. Different crystal phases[6,35] of this TMD compound have a great variety of potential applications in solar batteries,[36−41] sensors, and detectors[42−52] due to the high band-edge excitation of d−d transitions. Despite the continuously growing number of publications dedicated to MoS_2, some of its fundamental aspects still remain unclear. The aim of this work is to provide a convincing bonding picture for the MoS_2 monolayer.[53,54] In this paper, we perform the bonding analysis of this material and show that there are aromatic σ-bonds inside hexagonal rings. Mo atoms are the main carriers of this aromaticity.

2. COMPUTATIONAL METHODS

Solid-state calculations of the MoS_2 monolayer were performed within the density functional theory (DFT) formalism using the generalized gradient approximation with the Perdew−Burke−Ernzerhof exchange-correlation functional revised for solids (PBEsol)[55] and the projected augmented wave approach, as implemented in the Vienna Ab-initio Simulation Package (VASP).[56] The following lattice constants were used for the pristine MoS_2 unit cell (Figure 1): $a = b = 3.192$ Å, $c = 20.0$ Å, $\alpha = \beta = 90°$, $\gamma = 60°$.

The first step is preparatory calculations for bonding analysis performed using a $3 \times 3 \times 1$ supercell with a 350 eV kinetic energy cutoff and $11 \times 11 \times 1$ Γ-centered Monkhorst−Pack k-point sampling. The vacuum gap is added only in the z-direction, and the monolayer remains continuous. The unit cell of $3 \times 3 \times 1$ size is chosen for computational convenience. Then, periodic natural bond orbital (NBO)[57,58] and SSAdNDP[59−61] calculations were performed for the bonding analysis. Periodic NBO, like the standard NBO code, enables the assignment of 1c−2e bonds (lone pairs) and 2c−2e bonds (2-centered 2-electron bonds). The SSAdNDP code, which is an extension of AdNDP for solid-state calculations, allows the recognition of multicenter delocalized bonds (nc−2e, $n > 2$).

Received: January 19, 2020
Revised: February 22, 2020
Published: February 23, 2020

https://dx.doi.org/10.1021/acs.jpcc.0c00533
J. Phys. Chem. C 2020, 124, 6267−6273

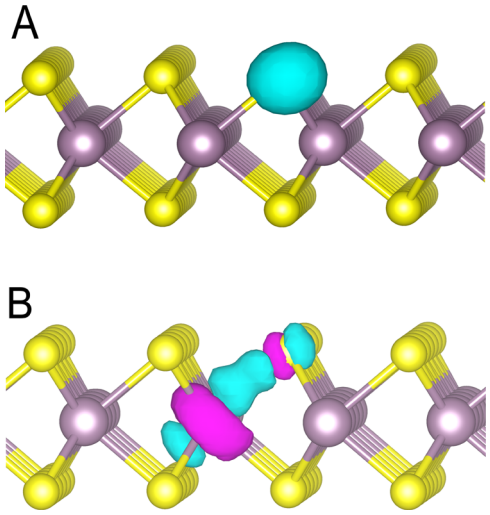

Figure 1. (A) 1c−2e s-lone pairs of S atoms, ONs = 1.9 |e|. (B) 2c−2e Mo−S bond, ONs = 1.8 |e|. Hereinafter, Mo atoms are purple, and S atoms are yellow.

AdNDP works within the concept of electron density overlapping. AdNDP, particularly SSAdNDP, was successfully applied as a bonding decoder to many one-dimensional (1D), two-dimensional (2D), and three-dimensional (3D) systems including those with aromatic properties.[62−73] Both NBO and AdNDP use the concept of occupation numbers (ONs), which represent the amount of electron density localized on a multicenter bond. The closer these values to 2.0, the more reliable a bonding picture is. A User-Directed Search procedure implemented in SSAdNDP (UD-SSAdNDP) allows solving nontrivial bonding cases. Comprehensive guidelines and examples to UD search can be found in the Supporting Information of the following literature.[74,75]

We chose the def2-TZVP[76] basis set for the projection of PW for the electron density matrix used in SSAdNDP calculations to be in precise agreement with the initial PW results.

The MN15L[77]/def2-TZVP level of theory was used for isolated cluster calculations via Gaussian16[78] software.

3. RESULTS AND DISCUSSION

Periodic NBO and SSAdNDP showed that as was expected, every Mo atom is bonded to six neighboring S atoms by 2-center−2-electron (2c−2e) bonds (Figure 1B) with ONs = 1.8 |e|. This implies that every S is bonded to three Mo atoms by 2c−2e bonds. Additionally, every sulfur has a lone pair (1c−2e) on it (Figure 1A) with ONs = 1.9 |e|. For the purpose of this work, we simplified the description of 2c−2e Mo−S bonds to the Lewis-like level. It does not affect in any way the main idea of the current paper − the presence of σ-aromaticity inside hexagonal rings. What matters is that every such 2c−2e bond requires 2 electrons as well as every lone pair. Therefore, after localization of all lone pairs and 2c−2e bonds 18 out of 162 valence electrons remain unlocalized in our unit cell. We tested 1c−1e bonds on S and 1c−2e bonds on Mo atoms in both spin-polarized and closed-shell configurations but occupation numbers (ONs) of such bonds are about 0.4−0.5 |e|, which does not look very convincing. This indicates the presence of conjugated multicenter bonds.

After testing several bonding combinations, we say without *a* shadow of *a* doubt that the MoS_2 monolayer possesses sigma aromaticity inside every hexagonal ring, that is, 3c−2e multicenter bonds over 3 Mo atoms with ONs being ∼1.5 |e| (Figure 2). As we can see in Figure 2, these sigma bonds in

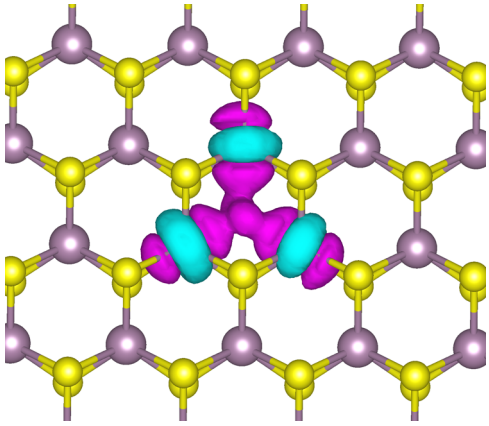

Figure 2. Sigma-aromatic orbital inside of the hexagonal MoS_2 ring.

some way consist of $3d_z^2$ molybdenum orbitals connected in the center of the ring. The σ-bonding is quite nontrivial since we observed that the major contribution to these σ-bonds comes from Mo atoms, i.e., when localizing conjugated orbitals like 9c−2e bonds over 3 molybdenum and 6 sulfur atoms, the ONs are just slightly higher being ∼1.6 |e|. Therefore, we refer these conjugated sigma systems as 3c−2e sigma bonds localized over Mo atoms. Alvarez et. al.[79] showed that Mo covalent radius is 1.54 Å, which, definitely, enables the overlapping of Mo electron density within the MoS_2 system.

It is worth mentioning that the energy difference between the closed- and open-shell configurations is just 5×10^{-8} eV according to our level of theory. Both configurations give absolutely the same bonding pattern.

The reader may set a fair point that the picture of the 3c−2e orbital is not very smooth. The problem likely lies in the periodic NBO projection code since d-metals like molybdenum are always tricky subjects in the field of quantum chemistry calculations. Indeed, the average value of the "spillover" output parameter of the projection code is 0.82, while its highest allowed value is 1.01. Once at least one of the spillover values exceeds this threshold, the results are not reliable anymore. Our value of 0.82 is below 1.01, so the results are trustworthy. However, based on our experience, when the system does not contain any d- or f- elements, the spillover values are of the order of $<10^{-3}$. That is why we assign the problem of the picture distortion to the interaction of d-electron density and projection code. Anyway, the code, definitely, works good enough for this system and qualitatively proves the presence of σ-aromaticity.

To further verify the presence of electron density inside the hexagonal ring, we performed Electron Localization Function (ELF) analysis. As can be seen in Figure 3, there is a trianglelike area of electron localization probability inside rings, which we interpret as the analog of the proposed delocalized σ-bond.

Thermal 2D-slices of ELF are presented in Figure 4. Noticeably, according to the thermal map, the highest ELF value inside the triangle area corresponds to the highest observable value around Mo atoms in all directions. This fact indicates that the remaining 18 electrons of the system indeed show delocalized behavior rather than lone pair character. The

https://dx.doi.org/10.1021/acs.jpcc.0c00533
J. Phys. Chem. C 2020, 124, 6267−6273

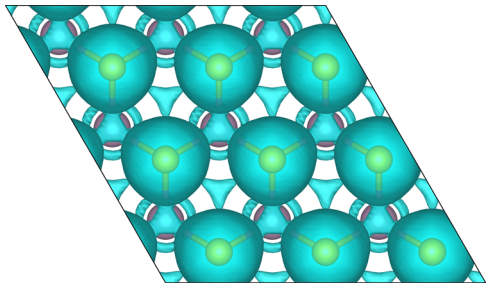

Figure 3. ELF of MoS_2. The isosurface value is 0.4.

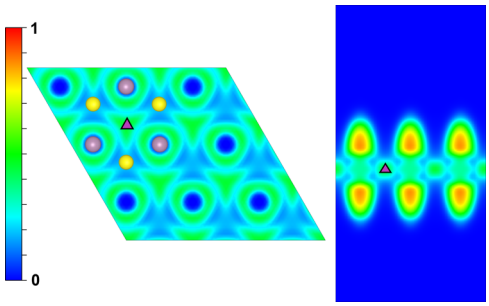

Figure 4. Left: ELF slice with 001 Miller indices; the sliced plane contains Mo atoms; three Mo and three S atoms are placed for convenience purposes. Right: ELF slice with 100 Miller indices. Purple triangles indicate the same point sliced in different directions.

above-mentioned trianglelike area is marked with purple triangles in Figure 4. For the reader's convenience, we indicated locations of Mo and S atoms in 2D-slices.

The analysis of the isolated cluster model is complicated by nontrivial periodic conditions; however, such complexity even supports our idea to some degree. Let us consider one solitary neutral ring with S atoms being bonded by Mo from all three directions (Figure 5). The system contains 72 valence

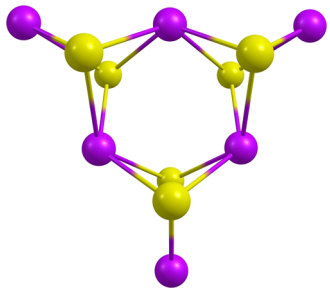

Figure 5. Isolated MoS_2 cluster model.

electrons. 48 of them are localized in a trivial way as six 1c−2e lone pairs on S and 18 2c−2e bonds between every S and Mo. Then, AdNDP reveals one lone pair on each Mo located on "triangle" vertices (Figure 6, left). No other lone pairs were found either on S or Mo as well as in solid-state calculations. Interestingly, we have found six 2c−2e bonds between Mo atoms with ONs = 1.8 |e| that form an outer frame (Figure 6, right). These six Mo−Mo bonds are likely to be formed by the electrons that molybdenum shares with sulfur in the periodic system. This fact once more indicates the strong electron density overlapping of Mo atoms.

66 electrons are localized to this point meaning that 6 electrons, or 3 bonds, remain unlocalized yet. For symmetry

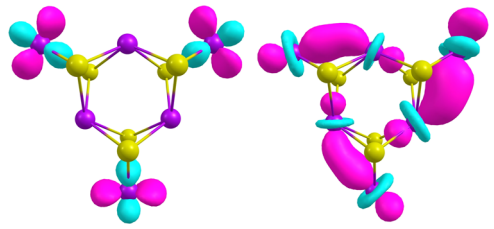

Figure 6. Left: three 1c−2e lone pairs on Mo atoms, ONs = 1.6. Right: 2c−2e Mo−Mo bonds; only 3 out of 6 are depicted for convenience purposes.

reasons, we initially tried to localize the remaining bonds over three triangles as shown in Figure 7 (left). 3c−2e localization over 3 Mo atoms is not very convincing with an ON of just 1.3 |e|. When the S atoms are treated alongside with Mo, that is, when the complete 5c−2e triangle is considered, the ON is increased to 1.6 |e|. However, the bond shape (see Supporting Information (SI), Figure S1) makes no sense in terms of potential periodic extension (Figure 9). Indeed, the 5c−2e bond expectedly disappears when a bigger cluster with more rings is considered (see SI, Figure S2) with the ON being reduced to 1.4 |e|.

The ON of the 3c−2e σ-bond inside the ring (Figure 8) is 1.8 |e|, and this bond does not break any symmetry and periodicity rules.

In addition, 4 electrons remain unlocalized yet. We believe that there is no way to localize them symmetrically because of the extremely complicated periodic conditions in the solid state, which are impossible to model within the isolated neutral cluster model. In qualitative approximation, every above-mentioned triangle (Figure 7) is a part of three neighboring hexagonal rings. Considering the presence of a 3c−2e σ-bond inside every ring, the triangle formally possesses 1/3 electron density of every σ-bond, i.e., 2/3 |e|. A schematic representation is given in Figure 7(right). In sum, there are $2/3 \times 3 = 2$ |e| on each triangle that came from three neighboring rings. In this cluster model, there are three triangles and only one ring. Roughly speaking, 2/3 |e| are withdrawn from each triangle to form one 3c−2e σ-bond inside *a* ring, while the remaining 4/3 |e| have nowhere to go due to the lack of periodicity. In total, $4/3 \times 3 = 4$ electrons remain unlocalizable since there are not enough rings in the isolated cluster model. The same bonding pattern is observed when a bigger cluster model is considered (Figure 9) with more unlocalizable bonds. Obviously, such an explanation aims at giving an understanding of why 4 electrons remain unlocalized rather than provide the physical insight into electron distribution.

The extended isolated cluster model (Figure 9) allows shedding some light on the 2c−2e bonding nature between Mo and S atoms. For example, let us consider the Mo atom, marked by a red circle in Figure 9, which experiences an approximated solid-state surrounding. According to the NBO analysis, it forms the following 2c−2e bonding combination with each S atom: 46% of electron density are attributed to Mo and 54% to S. 20% of molybdenum density are formed by p-electrons and 77% of d-electrons, while 18% of sulfur density comes from s-electrons and 81% from p-electrons. These numbers indicate that two-center bonding shows mostly covalent behavior between the d-electrons of molybdenum and the p-electrons of sulfur. However, sulfur forms 3 covalent bonds with neighboring molybdenum atoms but possesses 4 p-

https://dx.doi.org/10.1021/acs.jpcc.0c00533
J. Phys. Chem. C 2020, 124, 6267−6273

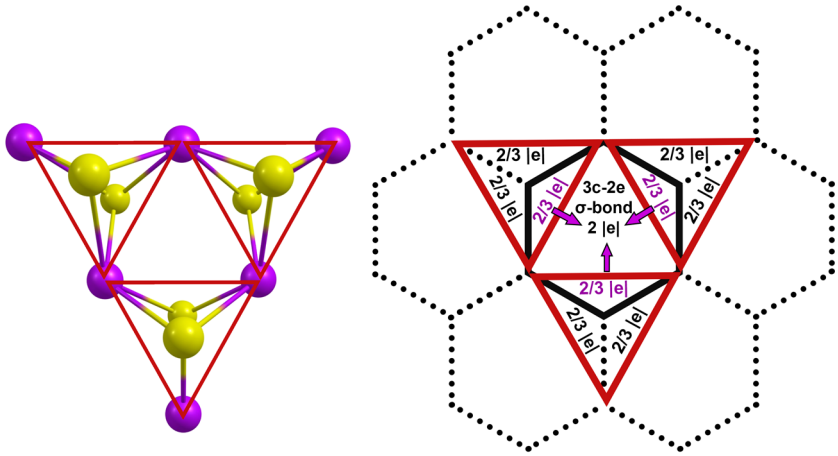

Figure 7. Left: Trianglelike structure of the MoS_2 isolated cluster. Right: schematic representation of σ-aromaticity electron distribution. Dotted lines indicate missing rings in the cluster model.

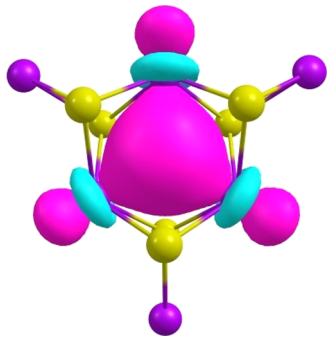

Figure 8. 3c−2e σ-aromatic bond inside the hexagonal ring. ON = 1.8 |e|.

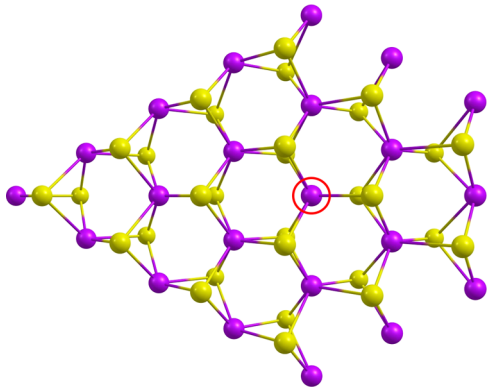

Figure 9. Extended isolated MoS_2 cluster model.

electrons. Interestingly, the NBO analyses in the cluster model show that the s-lone pair on sulfur is approximately 50% s-density and 50% p-density. These facts alongside with solid-state NBO charges, $Mo^{0.96+}S_2^{0.48-}$, and ELF analysis make reasonable the idea of covalent bonding between Mo and S, leaving the resonance interpretation possible, i.e., two single sulfur 3p-electrons interact with two Mo atoms through covalent bonds, and the paired 3p-electrons coordinate with one Mo atom that provides an empty orbital. Additionally, sulfur s-density is involved to a certain degree. As we can see, the 2c−2e bonding picture is complex in its electron involvement but can be simplified to the Lewis-like level.

The further discussion of the 2c−2e bonding nature is beyond the scope of the current research. As we mentioned above, what matters is electron counting. Indeed, the simplified Lewis-like bonding model via AdNDP is independent of the presence of any resonances and takes into account only electron counting.

4. CONCLUSIONS

As we found using the SSAdNDP approach, there are 2c−2e bonds between Mo and S as well as one lone pair on each S in the MoS_2 monolayer. Next, we found that the only way to localize the remaining electrons is to conjugate the 3c−2e σ-bonds inside every hexagonal ring. That is, three molybdenum atoms of every ring are the main carriers of the proposed σ-aromaticity. The Mo covalent radius of 1.54 Å enables electron density overlapping.

ELF analysis and the isolated cluster model support the idea of σ-aromaticity inside hexagonal rings as well as Mo−Mo electron density overlapping.

We believe that the deciphering of the MoS_2 monolayer bonding picture is an essential step toward understanding the nature of this unique and multifunctional material. We hope that our observation may shed light on some important aspects of molybdenum disulfide in the future.

■ ASSOCIATED CONTENT

Supporting Information

The Supporting Information is available free of charge at https://pubs.acs.org/doi/10.1021/acs.jpcc.0c00533.

Unit cell coordinates, cartesian coordinates of small and big clusters, and 5c−2e bond visualization (PDF)

■ AUTHOR INFORMATION

Corresponding Author

Alexander I. Boldyrev − *Department of Chemistry and Biochemistry, Utah State University, Logan 84322, Utah, United States;* orcid.org/0000-0002-8277-3669; Email: a.i.boldyrev@usu.edu

Author

Maksim Kulichenko − *Department of Chemistry and Biochemistry, Utah State University, Logan 84322, Utah, United States*

https://dx.doi.org/10.1021/acs.jpcc.0c00533
J. Phys. Chem. C 2020, 124, 6267−6273

Complete contact information is available at:
https://pubs.acs.org/10.1021/acs.jpcc.0c00533

Notes

The authors declare no competing financial interest.

■ ACKNOWLEDGMENTS

This work was supported by the USA National Science Foundation (grant CHEM-1664379) to AIB. The support and resources from the Centre for High Performance Computing at the University of Utah are gratefully acknowledged.

■ REFERENCES

(1) Rydberg, H.; Dion, M.; Jacobson, N.; Schröder, E.; Hyldgaard, P.; Simak, S. I.; Langreth, D. C.; Lundqvist, B. I. Van Der Waals Density Functional for Layered Structures. *Phys. Rev. Lett.* **2003**, *91*, No. 126402.

(2) Wang, Q. H.; Kalantar-Zadeh, K.; Kis, A.; Coleman, J. N.; Strano, M. S. Electronics and Optoelectronics of Two-Dimensional Transition Metal Dichalcogenides. *Nat. Nanotechnol.* **2012**, *7*, 699−712.

(3) Radisavljevic, B.; Radenovic, A.; Brivio, J.; Giacometti, V.; Kis, A. Single-Layer MoS_2 Transistors. *Nat. Nanotechnol.* **2011**, *6*, 147−150.

(4) Frindt, R. F.; Yoffe, A. D.; Bowden, F. P. Physical Properties of Layer Structures: Optical Properties and Photoconductivity of Thin Crystals of Molybdenum Disulphide. *Proc. R. Soc. London, Ser. A* **1963**, *273*, 69−83.

(5) Ruppert, C.; Aslan, O. B.; Heinz, T. F. Optical Properties and Band Gap of Single- and Few-Layer $MoTe_2$ Crystals. *Nano Lett.* **2014**, *14*, 6231−6236.

(6) Lv, R.; Robinson, J. A.; Schaak, R. E.; Sun, D.; Sun, Y.; Mallouk, T. E.; Terrones, M. Transition Metal Dichalcogenides and Beyond: Synthesis, Properties, and Applications of Single- and Few-Layer Nanosheets. *Acc. Chem. Res.* **2015**, *48*, 56−64.

(7) Elías, A. L.; Perea-López, N.; Castro-Beltrán, A.; Berkdemir, A.; Lv, R.; Feng, S.; Long, A. D.; Hayashi, T.; Kim, Y. A.; Endo, M.; et al. Controlled Synthesis and Transfer of Large-Area WS_2 Sheets: From Single Layer to Few Layers. *ACS Nano* **2013**, *7*, 5235−5242.

(8) Ghorbani-Asl, M.; Zibouche, N.; Wahiduzzaman, M.; Oliveira, A. F.; Kuc, A.; Heine, T. Electromechanics in MoS_2 and WS_2: Nanotubes vs. Monolayers. *Sci. Rep.* **2013**, *3*, No. 2961.

(9) Chen, R.; Zhao, T.; Wu, W.; Wu, F.; Li, L.; Qian, J.; Xu, R.; Wu, H.; Albishri, H. M.; Al-Bogami, A. S.; et al. Free-Standing Hierarchically Sandwich-Type Tungsten Disulfide Nanotubes/Graphene Anode for Lithium-Ion Batteries. *Nano Lett.* **2014**, *14*, 5899−5904.

(10) Luxa, J.; Mazánek, V.; Bouša, D.; Sedmidubský, D.; Pumera, M.; Sofer, Z. Graphene−Amorphous Transition-Metal Chalcogenide (MoS_x, WS_x) Composites as Highly Efficient Hybrid Electrocatalysts for the Hydrogen Evolution Reaction. *ChemElectroChem* **2016**, *3*, 565−571.

(11) Kim, J. Il.; Lee, B. S.; Chun, C.; Cho, J.-K.; Kim, S.-Y.; Song, S.-C. Long-Term Theranostic Hydrogel System for Solid Tumors. *Biomaterials* **2012**, *33*, 2251−2259.

(12) Alkis, S.; Öztaş, T.; Aygün, L. E.; Bozkurt, F.; Okyay, A. K.; Ortaç, B. Thin Film MoS_2 Nanocrystal Based Ultraviolet Photodetector. *Opt. Express* **2012**, *20*, 21815−21820.

(13) Hughbanks, T.; Hoffmann, R. Molybdenum Chalcogenides: Clusters, Chains, and Extended Solids. The Approach to Bonding in Three Dimensions. *J. Am. Chem. Soc.* **1983**, *105*, 1150−1162.

(14) Perea-López, N.; Elías, A. L.; Berkdemir, A.; Castro-Beltran, A.; Gutiérrez, H. R.; Feng, S.; Lv, R.; Hayashi, T.; López-Urías, F.; Ghosh, S.; et al. Photosensor Device Based on Few-Layered WS_2 Films. *Adv. Funct. Mater.* **2013**, *23*, 5511−5517.

(15) Zhan, Y.; Liu, Z.; Najmaei, S.; Ajayan, P. M.; Lou, J. Large-Area Vapor-Phase Growth and Characterization of MoS_2 Atomic Layers on a SiO2 Substrate. *Small* **2012**, *8*, 966−971.

(16) Xie, J.; Zhang, H.; Li, S.; Wang, R.; Sun, X.; Zhou, M.; Zhou, J.; Lou, X. W.; David; Xie, Y. Defect-Rich MoS_2 Ultrathin Nanosheets with Additional Active Edge Sites for Enhanced Electrocatalytic Hydrogen Evolution. *Adv. Mater.* **2013**, *25*, 5807−5813.

(17) Li, Y.; Wang, H.; Xie, L.; Liang, Y.; Hong, G.; Dai, H. MoS2 Nanoparticles Grown on Graphene: An Advanced Catalyst for the Hydrogen Evolution Reaction. *J. Am. Chem. Soc.* **2011**, *133*, 7296−7299.

(18) Splendiani, A.; Sun, L.; Zhang, Y.; Li, T.; Kim, J.; Chim, C.-Y.; Galli, G.; Wang, F. Emerging Photoluminescence in Monolayer MoS_2. *Nano Lett.* **2010**, *10*, 1271−1275.

(19) Pietrzyk, B.; Miszczak, S.; Kaczmarek, Ł.; Klich, M. Low Friction Nanocomposite Aluminum Oxide/MoS_2 Coatings Prepared by Sol-Gel Method. *Ceram. Int.* **2018**, *44*, 8534−8539.

(20) Colas, G.; Saulot, A.; Regis, E.; Berthier, Y. Investigation of Crystalline and Amorphous MoS_2 Based Coatings: Towards Developing New Coatings for Space Applications. *Wear* **2015**, *330*−*331*, 448−460.

(21) Li, X.; Zhu, H. Two-Dimensional MoS_2: Properties, Preparation, and Applications. *J. Materiomics* **2015**, *1*, 33−44.

(22) Ganatra, R.; Zhang, Q. Few-Layer MoS_2: A Promising Layered Semiconductor. *ACS Nano* **2014**, *8*, 4074−4099.

(23) Radisavljevic, B.; Whitwick, M. B.; Kis, A. Integrated Circuits and Logic Operations Based on Single-Layer MoS_2. *ACS Nano* **2011**, *5*, 9934−9938.

(24) Das, S.; Chen, H.-Y.; Penumatcha, A. V.; Appenzeller, J. High Performance Multilayer MoS_2 Transistors with Scandium Contacts. *Nano Lett.* **2013**, *13*, 100−105.

(25) Zhao, W.; Ribeiro, R. M.; Toh, M.; Carvalho, A.; Kloc, C.; Castro Neto, A. H.; Eda, G. Origin of Indirect Optical Transitions in Few-Layer MoS_2, WS_2, and WSe_2. *Nano Lett.* **2013**, *13*, 5627−5634.

(26) Schmidt, H.; Giustiniano, F.; Eda, G. Electronic Transport Properties of Transition Metal Dichalcogenide Field-Effect Devices: Surface and Interface Effects. *Chem. Soc. Rev.* **2015**, *44*, 7715−7736.

(27) Roldán, R.; Silva-Guillén, J. A.; López-Sancho, M. P.; Guinea, F.; Cappelluti, E.; Ordejón, P. Electronic Properties of Single-Layer and Multilayer Transition Metal Dichalcogenides MX_2 (M = Mo, W and X = S, Se). *Ann. Phys.* **2014**, *526*, 347−357.

(28) Komsa, H.-P.; Krasheninnikov, A. V. Electronic Structures and Optical Properties of Realistic Transition Metal Dichalcogenide Heterostructures from First Principles. *Phys. Rev. B* **2013**, *88*, 85318.

(29) Heine, T. Transition Metal Chalcogenides: Ultrathin Inorganic Materials with Tunable Electronic Properties. *Acc. Chem. Res.* **2015**, *48*, 65−72.

(30) Wang, H.; Yuan, H.; Sae Hong, S.; Li, Y.; Cui, Y. Physical and Chemical Tuning of Two-Dimensional Transition Metal Dichalcogenides. *Chem. Soc. Rev.* **2015**, *44*, 2664−2680.

(31) Chhowalla, M.; Liu, Z.; Zhang, H. Two-Dimensional Transition Metal Dichalcogenide (TMD) Nanosheets. *Chem. Soc. Rev.* **2015**, *44*, 2584−2586.

(32) Li, H.; Zhang, Q.; Yap, C. C. R.; Tay, B. K.; Edwin, T. H. T.; Olivier, A.; Baillargeat, D. From Bulk to Monolayer MoS_2: Evolution of Raman Scattering. *Adv. Funct. Mater.* **2012**, *22*, 1385−1390.

(33) Karunadasa, H. I.; Montalvo, E.; Sun, Y.; Majda, M.; Long, J. R.; Chang, C. J. A Molecular MoS_2 Mimic for Catalytic Hydrogen Generation. *Science* **2012**, *335*, 698−702.

(34) Hwang, H.; Kim, H.; Cho, J. MoS_2 Nanoplates Consisting of Disordered Graphene-like Layers for High Rate Lithium Battery Anode Materials. *Nano Lett.* **2011**, *11*, 4826−4830.

(35) He, Z.; Que, W. Molybdenum Disulfide Nanomaterials: Structures, Properties, Synthesis and Recent Progress on Hydrogen Evolution Reaction. *Appl. Mater. Today* **2016**, *3*, 23−56.

(36) Yue, G.; Lin, J.-Y.; Tai, S.-Y.; Xiao, Y.; Wu, J. A Catalytic Composite Film of MoS_2/Graphene Flake as a Counter Electrode for Pt-Free Dye-Sensitized Solar Cells. *Electrochim. Acta* **2012**, *85*, 162−168.

(37) Tsai, M.-L.; Su, S.-H.; Chang, J.-K.; Tsai, D.-S.; Chen, C.-H.; Wu, C.-I.; Li, L.-J.; Chen, L.-J.; He, J.-H. Monolayer MoS_2 Heterojunction Solar Cells. *ACS Nano* **2014**, *8*, 8317−8322.

https://dx.doi.org/10.1021/acs.jpcc.0c00533
J. Phys. Chem. C 2020, 124, 6267−6273

(38) Razzini, G.; Lazzari, M.; Bicelli, L. P.; Levy, F.; De Angelis, L.; Galluzzi, F.; Scafè, E.; Fornarini, L.; Scrosati, B. Electrochemical Solar Cells with Layer-Type Semiconductor Anodes. Performance of n-$MoSe_2$ Cells. *J. Power Sources* **1981**, *6*, 371−382.
(39) Gu, X.; Cui, W.; Li, H.; Wu, Z.; Zeng, Z.; Lee, S.-T.; Zhang, H.; Sun, B. A Solution-Processed Hole Extraction Layer Made from Ultrathin MoS_2 Nanosheets for Efficient Organic Solar Cells. *Adv. Energy Mater.* **2013**, *3*, 1262−1268.
(40) Gourmelon, E.; Lignier, O.; Hadouda, H.; Couturier, G.; Bernède, J. C.; Tedd, J.; Pouzet, J.; Salardenne, J. MS_2 (M = W, Mo) Photosensitive Thin Films for Solar Cells. *Sol. Energy Mater. Sol. Cells* **1997**, *46*, 115−121.
(41) Tai, S.-Y.; Liu, C.-J.; Chou, S.-W.; Chien, F. S.-S.; Lin, J.-Y.; Lin, T.-W. Few-Layer MoS_2 Nanosheets Coated onto Multi-Walled Carbon Nanotubes as a Low-Cost and Highly Electrocatalytic Counter Electrode for Dye-Sensitized Solar Cells. *J. Mater. Chem.* **2012**, *22*, 24753−24759.
(42) Wang, T.; Zhu, R.; Zhuo, J.; Zhu, Z.; Shao, Y.; Li, M. Direct Detection of DNA below Ppb Level Based on Thionin-Functionalized Layered MoS_2 Electrochemical Sensors. *Anal. Chem.* **2014**, *86*, 12064−12069.
(43) Loan, P. T. K.; Zhang, W.; Lin, C.-T.; Wei, K.-H.; Li, L.-J.; Chen, C.-H. Graphene/MoS_2 Heterostructures for Ultrasensitive Detection of DNA Hybridisation. *Adv. Mater.* **2014**, *26*, 4838−4844.
(44) Feng, Q.; Duan, K.; Ye, X.; Lu, D.; Du, Y.; Wang, C. A Novel Way for Detection of Eugenol via Poly (Diallyldimethylammonium Chloride) Functionalized Graphene-MoS_2 Nano-Flower Fabricated Electrochemical Sensor. *Sens. Actuators, B* **2014**, *192*, 1−8.
(45) Bissessur, R.; Schindler, J. L.; Kannewurf, C. R.; Kanatzidis, M. Nanoscale Composites Formed by Encapsulation of Polymers in MoS_2. From Conjugated Polymers to Plastics. Detection of Metal to Insulator Transition. *Mol. Cryst. Liq. Cryst. Sci. Technol., Sect. A* **1994**, *245*, 249−254.
(46) Farimani, A. B.; Min, K.; Aluru, N. R. DNA Base Detection Using a Single-Layer MoS_2. *ACS Nano* **2014**, *8*, 7914−7922.
(47) Wang, T.; Zhu, H.; Zhuo, J.; Zhu, Z.; Papakonstantinou, P.; Lubarsky, G.; Lin, J.; Li, M. Biosensor Based on Ultrasmall MoS_2 Nanoparticles for Electrochemical Detection of H_2O_2 Released by Cells at the Nanomolar Level. *Anal. Chem.* **2013**, *85*, 10289−10295.
(48) Kong, R.-M.; Ding, L.; Wang, Z.; You, J.; Qu, F. A Novel Aptamer-Functionalized MoS_2 Nanosheet Fluorescent Biosensor for Sensitive Detection of Prostate Specific Antigen. *Anal. Bioanal. Chem.* **2015**, *407*, 369−377.
(49) Wang, X.; Nan, F.; Zhao, J.; Yang, T.; Ge, T.; Jiao, K. A Label-Free Ultrasensitive Electrochemical DNA Sensor Based on Thin-Layer MoS_2 Nanosheets with High Electrochemical Activity. *Biosens. Bioelectron.* **2015**, *64*, 386−391.
(50) Miremadi, B. K.; Singh, R. C.; Morrison, S. R.; Colbow, K. A Highly Sensitive and Selective Hydrogen Gas Sensor from Thick Oriented Films of MoS_2. *Appl. Phys. A: Mater. Sci. Process* **1996**, *63*, 271−275.
(51) Kim, J.-S.; Yoo, H.-W.; Choi, H. O.; Jung, H.-T. Tunable Volatile Organic Compounds Sensor by Using Thiolated Ligand Conjugation on MoS_2. *Nano Lett.* **2014**, *14*, 5941−5947.
(52) Huang, J.; He, Y.; Jin, J.; Li, Y.; Dong, Z.; Li, R. A Novel Glucose Sensor Based on MoS_2 Nanosheet Functionalized with Ni Nanoparticles. *Electrochim. Acta* **2014**, *136*, 41−46.
(53) Jaramillo, T. F.; Jørgensen, K. P.; Bonde, J.; Nielsen, J. H.; Horch, S.; Chorkendorff, I. Identification of Active Edge Sites for Electrochemical H_2 Evolution from MoS_2 Nanocatalysts. *Science* **2007**, *317*, 100−102.
(54) Eknapakul, T.; King, P. D. C.; Asakawa, M.; Buaphet, P.; He, R.-H.; Mo, S.-K.; Takagi, H.; Shen, K. M.; Baumberger, F.; Sasagawa, T.; et al. Electronic Structure of a Quasi-Freestanding MoS_2 Monolayer. *Nano Lett.* **2014**, *14*, 1312−1316.
(55) Perdew, J. P.; Ruzsinszky, A.; Csonka, G. I.; Vydrov, O. A.; Scuseria, G. E.; Constantin, L. A.; Zhou, X.; Burke, K. Restoring the Density-Gradient Expansion for Exchange in Solids and Surfaces. *Phys. Rev. Lett.* **2008**, *100*, No. 136406.
(56) Kresse, G.; Hafner, J. Ab Initio Molecular Dynamics for Liquid Metals. *Phys. Rev. B* **1993**, *47*, 558−561.
(57) Glendening, E. D.; Reed, A. E.; Carpenter, J. E.; Weinhold, F. *NBO*, version 3.1.
(58) Carpenter, J. E.; Weinhold, F. Analysis of the Geometry of the Hydroxymethyl Radical by the "Different Hybrids for Different Spins" Natural Bond Orbital Procedure. *J. Mol. Struct.: THEOCHEM* **1988**, *169*, 41−62.
(59) Zubarev, D. Y.; Boldyrev, A. I. Developing Paradigms of Chemical Bonding: Adaptive Natural Density Partitioning. *Phys. Chem. Chem. Phys.* **2008**, *10*, 5207−5217.
(60) Zubarev, D. Y.; Boldyrev, A. I. Revealing Intuitively Assessable Chemical Bonding Patterns in Organic Aromatic Molecules via Adaptive Natural Density Partitioning. *J. Org. Chem.* **2008**, *73*, 9251−9258.
(61) Galeev, T. R.; Dunnington, B. D.; Schmidt, J. R.; Boldyrev, A. I. Solid State Adaptive Natural Density Partitioning: A Tool for Deciphering Multi-Center Bonding in Periodic Systems. *Phys. Chem. Chem. Phys.* **2013**, *15*, 5022−5029.
(62) Steglenko, D.; Minyaev, R. M.; Minkin, V. I.; Boldyrev, A. I. Difluorophosphorane-Flattened Phosphorene through Difluorination. *J. Phys. Chem. Lett.* **2018**, *9*, 6963−6966.
(63) Tkachenko, N. V.; Song, B.; Steglenko, D.; Minyaev, R. M.; Yang, L.-M.; Boldyrev, A. I. Computational Prediction of the Low-Temperature Ferromagnetic Semiconducting 2D SiN Monolayer. *Phys. Status Solidi B* **2019**, No. 1900619.
(64) Tkachenko, N. V.; Steglenko, D.; Fedik, N.; Boldyreva, N. M.; Minyaev, R. M.; Minkin, V. I.; Boldyrev, A. I. Superoctahedral Two-Dimensional Metallic Boron with Peculiar Magnetic Properties. *Phys. Chem. Chem. Phys.* **2019**, *21*, 19764−19771.
(65) Fedik, N.; Boldyrev, A. I.; Muñoz-Castro, A. Aromatic Character of $[Au_{13}]^{5+}$ and $[MAu_{12}]^{4+/6+}$ (M = Pd, Pt) Cores in Ligand Protected Gold Nanoclusters − Interplay between Spherical and Planar σ-Aromatics. *Phys. Chem. Chem. Phys.* **2019**, *21*, 25215−25219.
(66) Kulichenko, M.; Fedik, N.; Bozhenko, K. V.; Boldyrev, A. I. Inorganic Molecular Electride Mg4O3: Structure, Bonding, and Nonlinear Optical Properties. *Angew. Chem. Int. Ed.* **2019**, *25*, 5311−5315.
(67) Czekner, J.; Cheung, L. F.; Kocheril, G. S.; Kulichenko, M.; Boldyrev, A. I.; Wang, L.-S. High-Resolution Photoelectron Imaging of IrB_3^-: Observation of a π-Aromatic B_3^+ Ring Coordinated to a Transition Metal. *Angew. Chem. Int. Ed.* **2019**, *58*, 8877−8881.
(68) Boldyrev, A. I.; Kulichenko, M.; Fedik, N.; Muñoz-Castro, A. Expansion of Aromaticity Magnetic Criteria on Multi-Layer Structures. Magnetic Response and Spherical Aromaticity of Matryoshka-like $[Sn@Cu_{12}@Sn_{20}]^{12-}$ Cluster. *Chem. − Eur. J.* **2019**, DOI: 10.1002/chem.201905088.
(69) Kulichenko, M.; Fedik, N.; Steglenko, D.; Minyaev, R. M.; Minkin, V. I.; Boldyrev, A. I. Periodic F-Defects on the MgO Surface as Potential Single-Defect Catalysts with Non-Linear Optical Properties. *Chem. Phys.* **2020**, *532*, No. 110680.
(70) Fedik, N.; Kulichenko, M.; Steglenko, D.; Boldyrev, A. I. Can Aromaticity Be a Kinetic Trap? Example of Mechanically Interlocked Aromatic [2-5]Catenanes Built from Cyclo[18]Carbon. *Chem. Commun.* **2020**, DOI: 10.1039/C9CC09483K.
(71) Fedik, N.; Boldyrev, A. I. Insight into The Nature of Rim bonds in Coronene. *J. Phys. Chem A* **2018**, *122*, 8585−8590.
(72) Liu, G.; Fedik, N.; Martinez-Martinez, C.; Ciborowski, S. M.; Zhang, X.; Boldyrev, A. I.; Bowen, K. H. Realization of Lewis Basic Sodium Anion in the NaBH3- cluster. *Angew. Chem. Int. Ed.* **2019**, *58*, 13789−13793.
(73) Gapurenko, O. A.; Minyaev, R. M.; Fedik, N. S.; Koval, V. V.; Boldyrev, A. I.; Minkin, V. I. Structure and bonding of new boron and carbon superpolyhedra. *Struct. Chem.* **2019**, *30*, 805−814.
(74) Kulichenko, M.; Fedik, N.; Bozhenko, K. V.; Boldyrev, A. I. Hydrated Sulfate Clusters $SO_4^{2-}(H_2O)_n$ (n = 1−40): Charge Distribution Through Solvation Shells and Stabilization. *J. Phys. Chem. B* **2019**, *123*, 4065−4069.

(75) Fedik, N.; Kulichenko, M.; Boldyrev, A. I. Two Names of Stability: Spherical Aromatic or Superatomic Intermetalloid Cluster $[Pd_3Sn_8Bi_6]^{4-}$. *Chem. Phys.* **2019**, *522*, 134−137.
(76) Dunning, T. H. Gaussian Basis Sets for Use in Correlated Molecular Calculations. I. The Atoms Boron through Neon and Hydrogen. *J. Chem. Phys.* **1989**, *90*, 1007−1023.
(77) Yu, H. S.; He, X.; Truhlar, D. G. MN15-L: A New Local Exchange-Correlation Functional for Kohn−Sham Density Functional Theory with Broad Accuracy for Atoms, Molecules, and Solids. *J. Chem. Theory Comput.* **2016**, *12*, 1280−1293.
(78) Frisch, M. J.; Trucks, G. W.; Schlegel, H. B.; Scuseria, G. E.; Robb, M. A.; Cheeseman, J. R.; Scalmani, G.; Barone, V.; Petersson, G. A.; Nakatsuji, H.; Li, X.; Caricato, M.; Marenich, A. V.; Bloino, J.; Janesko, B. G.; Gomperts, R.; Mennucci, B.; Hratchian, H. P.; Ortiz, J. V.; Izmaylov, A. F.; Sonnenberg, J. L.; Williams-Young, D.; Ding, F.; Lipparini, F.; Egidi, F.; Goings, J.; Peng, B.; Petrone, A.; Henderson, T.; Ranasinghe, D.; Zakrzewski, V. G.; Gao, J.; Rega, N.; Zheng, G.; Liang, W.; Hada, M.; Ehara, M.; Toyota, K.; Fukuda, R.; Hasegawa, J.; Ishida, M.; Nakajima, T.; Honda, Y.; Kitao, O.; Nakai, H.; Vreven, T.; Throssell, K.; Montgomery, J. A.; Peralta, J. E., Jr.; Ogliaro, F.; Bearpark, M. J.; Heyd, J. J.; Brothers, E. N.; Kudin, K. N.; Staroverov, V. N.; Keith, T. A.; Kobayashi, R.; Normand, J.; Raghavachari, K.; Rendell, A. P.; Burant, J. C.; Iyengar, S. S.; Tomasi, J.; Cossi, M.; Millam, J. M.; Klene, M.; Adamo, C.; Cammi, R.; Ochterski, J. W.; Martin, R. L.; Morokuma, K.; Farkas, O.; Foresman, J. B.; Fox, D. J.. *Gaussian 16*, revision B.01; Gaussian, Inc.: Wallingford CT, 2016.
(79) Cordero, B.; Gómez, V.; Platero-Prats, A. E.; Revés, M.; Echeverría, J.; Cremades, E.; Barragán, F.; Alvarez, S. Covalent Radii Revisited. *Dalton Trans.* **2008**, *40*, 2832−2838.

https://dx.doi.org/10.1021/acs.jpcc.0c00533
J. Phys. Chem. C 2020, 124, 6267−6273